Simultaneous Measurements of Electric and Thermal Fields Utilizing an Electrooptic Semiconductor Probe

Ronald M. Reano, *Student Member, IEEE*, Kyoung Yang, *Member, IEEE*, Linda P. B. Katehi, *Fellow, IEEE*, and John F. Whitaker, *Member, IEEE*

***Abstract*—A method to simultaneously measure electric and thermal fields with a single probe is presented in this paper. The Pockels effect is employed within a gallium–arsenide probe to measure electric fields, and the effect of photon absorption due to bandtail states in the semiconductor is used to determine temperature. The measured optical power is found to be inversely related to temperature, in agreement with theory, and experimental results demonstrate a temperature sensitivity of 0.31 μW/°C at 25 °C and an accuracy of ±0.5 °C between 20 °C–60 °C. The minimum detectable electric field is 1.24±0.06 V/m using a 300-ms electrical bandwidth. Temporal phase stability of ±3°/h is achieved through the implementation of a system phase reference channel. The invasiveness of the probe is quantified by examining the change in the characteristic impedance and capacitance per unit length of a planar transmission line. Measured and simulated data show that the effect is equivalent to a lumped shunt capacitance on the order of a few femtofarads. The examination of a monolithic microwave integrated circuit in an X-band quasi-optical power-combining array and the calibration of electric-field data that was corrupted by temperature-dependent effects inherent to the electrooptic probe demonstrate the capability of this combined electrothermal measurement technique.**

***Index Terms*—Electrooptic effects, electrothermal effects, optoelectronic devices, semiconductor materials.**

I. Introduction

THE electrothermal behavior of active microwave and millimeter-wave circuits has received growing attention in recent years [1]–[3]. The thermal characteristics become especially important in active antenna arrays and quasi-optical power-combining structures where a multitude of biased monolithic microwave integrated circuits (MMICs) are in close proximity. The generation of heat in such configurations mandates a strong consideration of heat dissipation in the overall design [4], [5].

Several methods have been developed to characterize and diagnose the behavior of such circuits. To examine the electrical behavior, optical techniques such as those that use electrooptic probes for the noncontact field mapping of electric fields have been employed [6], [7]. Separate methods exist for observing thermal effects including the use of thermal cameras, IR microscopes, thermocouples, and thermistors.

A major factor that has yet to be considered when applying electrooptic field-mapping techniques to the characterization of active microwave circuits is the temperature dependence of the probe itself. The electrooptic coefficients that govern the response of the probe to RF fields are known to vary with temperature [8]. Additionally, in III–V semiconductor-based probes, the temperature dependence of the optical absorption edge is significant. The sensitivity of the absorption edge to temperature has been used, for example, to monitor the temperature in indium–phosphide-based semiconductor substrates where knowledge of the epitaxial growth temperature is critical [9].

This paper addresses the temperature-dependent effects associated with gallium–arsenide electrooptic probes and presents a full characterization of a field-mapping system. From this study, it is shown that both electric and thermal fields can be measured simultaneously. This allows for the combined electrothermal examination of active microwave and millimeter-wave circuits with a single probe and the ability to calibrate electric field data that is corrupted when the probe is placed in areas where temperature variations are present. Techniques for scaling relative electric-field measurements to absolute units and for stabilizing electric-field phase drift are also presented. Finally, the probe invasiveness on a planar transmission line is quantified by investigating the change in the characteristic impedance and capacitance per unit length as the probe is brought into the near field. Sample measurements of a quasi-optical power-combining array demonstrate the usefulness of this novel electrothermal measurement system.

II. Theory

The physical mechanisms employed to measure temperature are the temperature dependence of the energy bandgap in intrinsic semiconductors and its effect on the absorption of optical power. The following is a well-known equation describing this phenomena, as established by Varshni [10]:

$$E_g(T) = E_g(0) - \frac{\gamma T^2}{T+\beta} \tag{1}$$

where γ and β are material-specific empirical constants, $E_g(T)$ is the bandgap energy at temperature T, and $E_g(0)$ is the bandgap energy at 0 K. For photon energies in the bandgap and near the band edge, the absorption coefficient α has been found

Manuscript received March 31, 2001; revised August 24, 2001. This work was supported by the Multidisciplinary University Research Initiative on Spatial and Quasi-Optical Power Combining monitored by the Army Research Office Grant DAAG 55-97-0132 under subcontract to Clemson University.

The authors are with the Center for Ultrafast Optical Science and Radiation Laboratory, Department of Electrical Engineering and Computer Science, The University of Michigan at Ann Arbor, Ann Arbor, MI 48109-2122 USA (e-mail: whitaker@umich.edu).

Publisher Item Identifier S 0018-9480(01)10434-5.

to decay exponentially with decreasing photon energy $h\nu$ due to the presence of bandtail states. The dependence on photon energy is shown to follow [11]

$$\alpha = A\exp\left[(h\nu - x_o)/y_o)\right] \tag{2}$$

where A, x_o, and y_o are constant curve-fitting parameters at 300 K. For GaAs at room temperature ± 70 K, the bandgap and absorption coefficient variation with temperature can be linearized to within 5%. Linearizing (1) and (2) about a nominal temperature T_o and photon energy $(h\nu)_o$ and noting that

$$\frac{\partial\alpha}{\partial(h\nu)} = \xi\frac{\partial\alpha}{\partial E_g} \tag{3}$$

where ξ is a constant on the order of one for the temperature range of interest, the flow of optical power P through the semiconductor is found to obey the following temperature dependence:

$$\frac{1}{P} \propto 1 + \kappa T \tag{4}$$

where κ is a constant that depends on the dimension of the semiconductor in the direction of propagation. Therefore, by monitoring the absorption response of an optical beam that is directed to propagate through a section of semiconducting material, the change in temperature can be inferred in a manner that is linear with the inverse of optical power.

To simultaneously measure electric fields, the semiconductor must also be electrooptic. Due to the Pockels effect, an optical beam propagating through an electrooptic material exhibits a change in polarization state when the material is in the presence of an externally applied, and relatively low-frequency electric field. The change in polarization state can be made to result in an amplitude modulation of the optical beam that is proportional to the intensity of the applied electric field. The optical transmission T_o through an electrooptic modulator set up for 50% transmission is given by [8]

$$T_o = \sin^2\left[\frac{1}{2}\left(\frac{\pi}{2} + \pi\frac{E_{\rm rf}d}{V_\pi}\sin(\omega_{\rm rf}t + \phi_{\rm rf})\right)\right] \tag{5}$$

where $E_{\rm rf}$ is the average RF electric-field magnitude induced in the probe, $\phi_{\rm rf}$ is the RF electric-field phase, d is the crystal thickness along the direction of propagation of the optical beam, $\omega_{\rm rf}$ is the RF frequency, t is time, and V_π is the half-wave voltage of the electrooptic material. For $E_{\rm rf}d \ll V_\pi$, the intensity modulation is linear with the average RF electric field induced across the probe.

III. Implementation

The experimental setup is shown in Fig. 1. The probe material is <100> GaAs with a normal-surface area of 500 μm $\times$ 500 μm and a vertical thickness of 200 μm. A Ti : sapphire laser tuned to 895 nm is used to generate a linearly polarized sampling beam that is coupled to the probe via a section of single-mode optical fiber and a graded-index lens [12]. Appropriate phase retarders are placed to configure a 50% transmission intensity modulator for electric-field measurements.

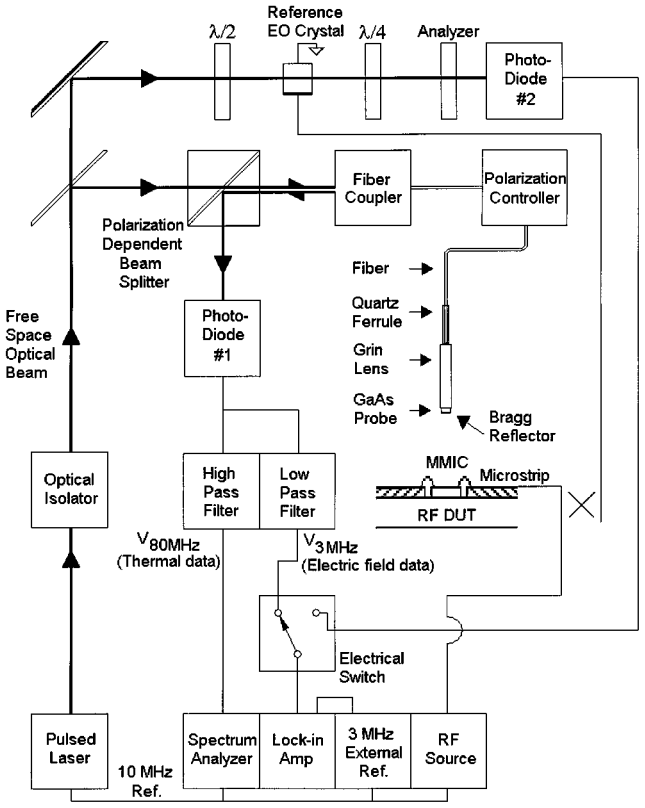

Fig. 1. Experimental setup for combined electrothermal measurements. By separating the electric field and temperature signals in frequency, both may be acquired with a single probe. The top beam line is implemented for system phase stability. The example RF DUT in this figure is a MMIC with a microstrip feed.

To alleviate the need for a fast photodetector, and to provide a method by which the phase of a signal may also be easily sensed, the device under test is fed via an RF synthesizer configured for harmonic mixing in order to down convert the sampled electric fields to IF frequencies. This is accomplished by mode locking the laser to produce a train of 80-fs pulses at a pulse repetition rate of 80 MHz and setting the RF source frequency to an integer multiple of the pulse repetition rate, plus an offset that corresponds to the IF frequency. An IF frequency of 3 MHz is used and was selected based on a tradeoff consideration between signal-to-noise degradation due to $1/f$ noise at lower IF frequencies and the loss of sensitivity incurred by selecting higher IF frequencies. Since the 80-MHz component is not modulated coherently, its amplitude does not change as it passes through the electrooptic crystal.

A photodiode functions as an envelope detector that transforms the 3-MHz modulation and the 80-MHz pulse-repetition component to electrical signals for detection. The 3-MHz signal, denoted $V_{3\ \rm MHz}$, is the modulation signal that provides the electric-field information and the 80-MHz signal, denoted $V_{80\ \rm MHz}$, is the spectral component that is monitored for temperature measurements. A high-pass filter that filters as an open-circuit couples the 80-MHz pulse-repetition component to a spectrum analyzer while the 3-MHz modulation signal is coupled to a lock-in amplifier with a low-pass filter that filters as an open-circuit for the 80-MHz signal. Such an arrangement allows for the simultaneous measurement of thermal and electric fields.

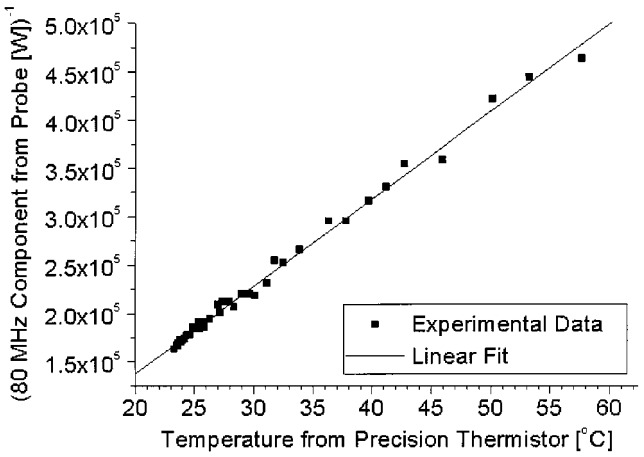

Fig. 2. Temperature response of the GaAs probe.

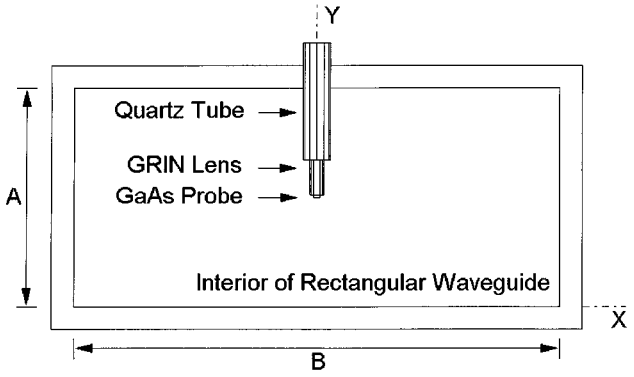

Fig. 3. Cross-sectional view of the configuration used to scale relative electric-field measurements to absolute units (i.e., volts/meter). The probe is inserted into a rectangular waveguide and analytical expressions are used to relate the electrooptic signal to the RF input power.

IV. Characterization

A. Thermal Response

To characterize the thermal properties of the electrooptic sensor, the probe was mounted in still air approximately 4 in above a hotplate. A precision thermistor with a tolerance of ± 0.2 °C was positioned adjacent to the probe to monitor the temperature variations of the ambient air as the hot plate was turned on and off. Absorption data from the probe and temperature data from the thermistor were collected over a 50-min period as the temperature was varied between 20 °C–60 °C. The results are shown in Fig. 2 and agree with the theory as described in (4).

The temperature accuracy and sensitivity of the probe are determined from a linear regression analysis of the data shown in Fig. 2. The accuracy, calculated from the standard deviation of the data set composed of the absolute value of the deviations from the linear fit, is calculated to be ± 0.5 °C. Using the thermistor resistance versus temperature characteristic and the observed relationship between the measured optical power and thermistor resistance, the sensitivity is calculated to be equal to 0.31 μW/°C at 25 °C.

B. Absolute Electric-Field Magnitude

The output of the lock-in amplifier is a dc voltage that is proportional to the first harmonic rms amplitude of the RF modulation signal. Although this scheme is useful for relative electric-field measurements, scaling the output to electric field units (i.e., volts/meter) is desirable in order to obtain absolute average field measurements and to characterize the dynamic range of the system. A direct determination of the proportionality constant relating the output of the lock-in amplifier and $E_{\rm rf}d$ would allow the output to be scaled to absolute units. However, this would require an accurate characterization of the power mismatches presented by the fiber coupler, the interface between the fiber and the grin lens, the interface between the grin lens and the GaAs probe, and the reflectivity of the Bragg reflector.

To circumvent these practical difficulties, an alternative method for scaling the measured data to absolute units has been developed. This method involves placing the probe in a region where the absolute value of the electric-field distribution is known. The region inside of a shorted rectangular waveguide enclosure was selected due to the simplicity of the analytical closed-form field solutions, the confinement of the fields within a closed structure, and the direct relationship between the power input into the waveguide and the absolute magnitude of the electric field. Previous investigators have scaled electrooptic signals to RF electromagnetic fields associated with open structures such as microstrip and coplanar waveguide lines in order to determine minimum detectable signal levels [7], [13]. The method presented here, however, involves a completely enclosed structure. Relating input RF power to expected fields over an open structure such as microstrip or coplanar waveguide (CPW) leads to inaccuracies due to losses associated with radiation, losses associated with the coax-to-microstrip/CPW transitions, the sensitivity in the positioning of the probe above the line (due to exponentially decaying fields), and the need to rely on nonclosed-form solutions of the microstrip/CPW fields. The approach presented in this paper is also independent of the height of the crystal above a device-under-test (DUT) since the procedure directly scales the amplitude measurement on the RF lock-in with the induced optical retardation.

The geometry of the insertion of the probe into the rectangular waveguide is shown in Fig. 3. In the absence of the probe, the magnitude of the electric field at a standing wave peak $|E_{\rm peak}|$ can be related to the input power P via the wave equation and the Poynting vector as

$$|E_{\rm peak}| = \sqrt{\frac{16P\omega\mu_o}{k_z AB}} \quad k_z = \sqrt{\omega^2\mu_o\varepsilon_o - \left(\frac{\pi}{B}\right)} \qquad (6)$$

where ω is the radian frequency, μ_o is the free-space permeability, ε_o is the free-space permittivity, k_z is the phase constant along the direction of propagation, A is the length of the short edge of the rectangular waveguide, and B is the length of the long edge. Since each quantity on the right-hand side of the equation for $|E_{\rm peak}|$ is measurable, the expected value for the magnitude of the electric field at a standing-wave peak can be determined.

A complication is the distortion of the electric field due to the presence of the probe in the waveguide. Since the graded-index lens self-focuses the optical beam to a beam waist of less than

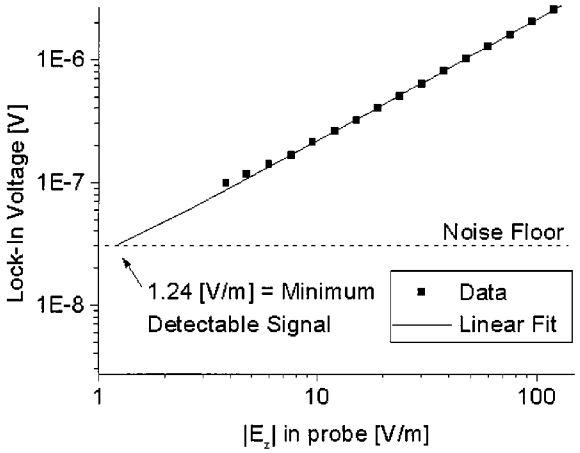

Fig. 4. Measurement linearity and minimum detectable electric field. Over a 300-ms bandwidth, the electrooptic signal reaches the noise floor at 1.24 V/m.

10 μm, the field internal to the probe within a 10-μm-diameter cylinder centered between the top and bottom faces of the probe is the region of interest. For frequencies such that the guide wavelength is much larger than the probe dimensions, a quasi-static approximation bounds the electric field inside the probe $E_{\rm int}$ to

$$\frac{1}{\varepsilon_{rp}} E_{\rm ext} < E_{\rm int} < E_{\rm ext} \tag{7}$$

where $E_{\rm ext}$ is the field in the absence of the probe and ε_{rp} is the dielectric constant of the probe [14]. The relation in (7) holds because the probe appears as a dielectric object that is neither a thin slab, nor a long thin cylinder. A full-wave finite-element-method-based simulation based on the geometry in Fig. 3 was employed to analyze the expected ratio of $E_{\rm int}$ to $E_{\rm ext}$.[1] The average electric-field induced in the probe is found to be 19% of the electric field when the probe is absent. This factor is taken into account when scaling relative measurements to volts/meter via (6).

The measured results for the probe in the waveguide are shown in Fig. 4. For this experiment, a shorted WR-137 waveguide (height $A = 15.8$ mm, width $B = 34.9$ mm) was employed and the operating frequency was set to 6.963 GHz. The waveguide short was coupled to the RF synthesizer via a coaxial cable and coax-to-waveguide adapter. An RF power meter was used to measure the input power going into the waveguide from the coax-to-waveguide adapter. The mismatch at the coax-to-waveguide transition was characterized via time-domain (bandpass) measurements on a vector network analyzer. The peak return loss at the coax-to-waveguide transition was -29 dB below the peak return loss at the waveguide short. Therefore, the transition mismatch can be neglected with negligible error. As shown in Fig. 4, the lock-in voltage can be scaled to average volts/meter in a linear fashion. By stepping down the input power, the minimum detectable average electric field inside of the probe is 1.24 V/m. A measurement error of ± 0.06 V/m is estimated from consideration of the measurement error of the power meter, positioning error of the probe within the waveguide, convergence error associated with the ratio of $E_{\rm int}$ to $E_{\rm ext}$, and the error in the linear fit of the data extrapolated to the noise floor.

To state a sensitivity for the system, knowledge of the system bandwidth is required. Since a lock-in amplifier is employed in the last stage, the system bandwidth is determined by the time constant on the output *RC* circuit. For the measurements shown in Fig. 4, the time constant was 300 ms. Therefore, the sensitivity of the system is 0.68 ± 0.03 V/m/$\sqrt{\rm Hz}$. This value is useful as a figure-of-merit, but should be interpreted with caution. In particular, it is dependent on the intensity of the input optical beam imposed on the electrooptic crystal. The maximum input power of the optical beam that can be coupled into the fiber is limited to 20 mW in order to avoid two-photon absorption in the GaAs. The actual optical power that reaches the probe tip is dependent on the system optical alignment, which is dominated by the coupling of the free-space beam into the optical fiber via the fiber coupler. To date, 0.68 V/m/$\sqrt{\rm Hz}$ is the highest sensitivity that this system has demonstrated.

C. Temporal Stabilization of Electric-Field Phase

An external 40-MHz crystal oscillator serves as the master phase synchronization signal for the entire system. This oscillator is frequency multiplied to 80 MHz to provide external feedback to the Ti : sapphire-laser pulse repetition rate and frequency divided by ten in order to provide a common 10-MHz reference signal for the external 3-MHz lock-in reference and the RF synthesizer. In principle, the modulation on the 80-MHz pulse train will be phase synchronized with the 3-MHz reference oscillator allowing phase measurements of the electric field. Observations of the measured phase stability over time, however, have produced results that demonstrate a consistent phase drift in the system.

In order to correct for the phase drift, a reference electrooptic signal has been integrated into the system. A key point regarding this method of phase stabilization is that it corrects for phase drift regardless of the source of phase instability (whether it be due to a single component of the system or due to a combination of components). As shown in Fig. 1, a beam splitter is used to couple 30% of the free space optical beam to a beam-line consisting of a half-wave plate, an electrooptic probe crystal, a quarter-wave plate, a polarizer, and a second photodiode. The optical elements are configured to produce 50% transmission intensity modulation of the optical beam in response to an RF modulating signal, which is coupled off from the RF source feeding the DUT. An electrical switch is employed to toggle between the photodiode that collects data from the DUT and the photodiode that collects data from the reference crystal.

By using the phase reference channel, the system phase drift can be calibrated out. A demonstration of the effect of the phase calibration is shown in Fig. 5. The reference electrooptic crystal was bismuth silicate (BSO), although any electrooptic crystal with a sufficient $n^3 r$ parameter will suffice, and the modulating signal was imposed on the crystal via a horn antenna (8.003 GHz RF) for simplicity. The probe was kept stationary above the DUT while phase data was toggled between photodiode #1 and photodiode #2 every 10 s. Over a 60-min time interval, the uncalibrated phase data from photodiode #1 happened to drift from 49° to -8°. This data represents an intermittent system temporal

[1]Maxwell HFSS Release 6, Ansoft, Pittsburgh, PA, 1998.

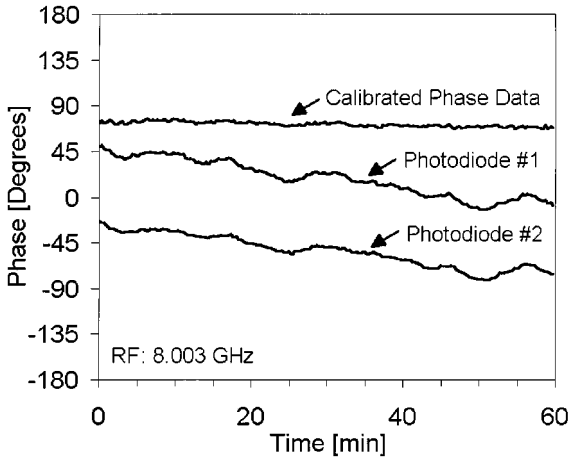

Fig. 5. Measured phase drift and demonstration of correction. Any drift in the measurement of electric-field phase is stabilized via the implementation of a phase reference channel. The calibrated phase data, taken over 1 h, has a standard deviation of $\pm 3^{\circ}$.

phase instability. The phase data from the reference channel is seen to drift along with the data from the DUT. Subtracting the phase drift in the uncalibrated data results in the calibrated data set, which shows a standard deviation of $\pm 3^{\circ}$ over the 60-min time interval.

V. Invasiveness

A. Simulations

The DUT that is selected for the study of probe invasiveness is a CPW transmission line. The choice of the CPW line as the DUT allows the invasiveness of the probe to be quantified in terms of the characteristic impedance of the line and the capacitance per unit length. When the probe is placed in close proximity to the DUT, two undesirable effects occur. First, the DUT is electromagnetically perturbed and, second, the sampled electric field present in the probe is distorted. The first effect is examined in this paper. The second effect has been examined in the time domain where electric fields generated on a CPW line due to the propagation of sub-picosecond pulses have been analyzed [15], [16]. It was found that, due to strong dispersion above 0.6 THz, the sampled signal field in the probe can be significantly different from the unprobed field. In the spectral domain, however, where the fields are mapped spatially at a single frequency, measurements of the sampled field inside of the probe have demonstrated spatial measurements that are in good agreement with both analytical and simulated field solutions [12], [17].

The invasiveness of dielectric probes over transmission lines, in terms of S_{11}, was studied via finite-difference-time-domain simulations in [18], by a two-dimensional (2-D) quasi-static field analysis based on a TEM-mode assumption in [19], and experimentally in terms of time-delayed pulses in [20]. In this paper, we quantify invasiveness in terms of the spatial perturbation in the characteristic impedance and capacitance per unit length of a CPW line with the probe present via a quasi-static field analysis based on field solutions from three-dimensional full-wave finite-element-method simulations. This method is applied at 10 GHz and is applicable at low microwave frequencies where the imaginary part of the characteristic impedance is relatively small. At higher frequencies, the imaginary part of the characteristic impedance becomes appreciable due to space and surface wave radiation [21]. Supporting measurements in the time and frequency domains follow the simulations.

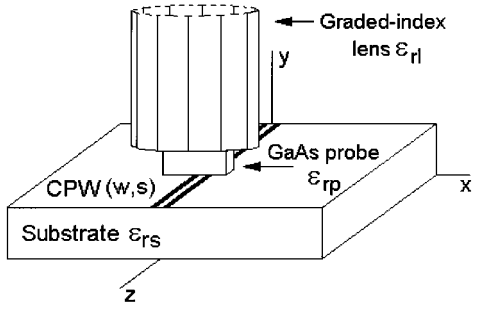

Fig. 6. Full-wave simulation geometry for the examination of invasiveness of the probe on a DUT. In this case, the DUT is a CPW with lateral dimensions less than the footprint of the probe.

The geometry of the simulation is shown in Fig. 6. Although the transverse orthogonal refractive indexes in the electrooptic probe vary in time with the presence of an RF electric field, an index ellipsoid analysis verifies that the change is much less than a fraction of a percent at breakdown fields. Therefore, with negligible error, the electrooptic probe is modeled with a constant dielectric permittivity and a linear electromagnetic simulator is utilized.

Given the electric-field solution in the region of the probe, a quasi-static analysis is performed to determine the charge per unit length, capacitance per unit length, and characteristic impedance versus distance along the direction of propagation. This is valid since the phase in any transverse (xy) plane is essentially constant. The charge per unit length Q_l along the transmission line can be determined as a function of distance as

$$Q_\ell(z) = \varepsilon \oint_{c(z)} \overrightarrow{E} \cdot d\overrightarrow{\ell} \text{ C/m} \tag{8}$$

where the integral is evaluated in the transverse plane and the contour encloses the center conductor of the transmission line. As long as the contour of integration is selected sufficiently near the conductor, the longitudinal electric-field component will be sufficiently small compared to the transverse components allowing a charge per unit length to be evaluated with a line integral. The capacitance per unit length C_l and characteristic impedance of the transmission line Z_o are obtained from

$$C_\ell(z) = \frac{Q_\ell(z)}{V(z)} \text{ F/m}$$
$$V(z) = \int_1^2 \overrightarrow{E} \cdot d\overrightarrow{\ell} \text{ V} \tag{9}$$

$$Z_o(z) = \sqrt{\frac{L_\ell}{C_\ell}} = \frac{1}{c}\sqrt{\frac{1}{C_{\ell,\varepsilon_s=\varepsilon_o}(z) \cdot C_\ell(z)}} \tag{10}$$

where $V(z)$ is the voltage between conductors, L_l, is the inductance per unit length, c is the speed of light in vacuum, and $C_{l,\varepsilon_s=\varepsilon_o}$ is the capacitance per unit length for a vacuum-filled transmission line.

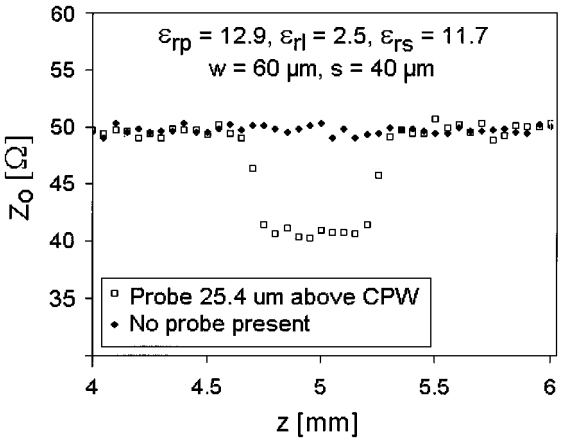

Fig. 7. Simulation results of the spatial extent of the perturbation of the characteristic impedance Z_o of the CPW. The presence of the probe changes Z_o by 19% when the bottom edge of the probe is 25.4 μm above the surface of the transmission line. The full-width at half-maximum of the perturbation is 0.5 mm and is equal to the length of the probe.

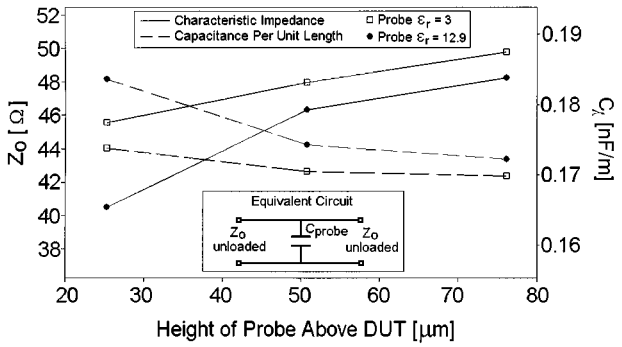

Fig. 8. Sensitivity analysis of invasiveness simulations. Results show that, as the height of the probe becomes less than 50 μm, the change in Z_o and the capacitance per unit length become significant. In practice, there is a tradeoff between invasiveness and signal-to-noise. The effect of the probe is equivalent to a lumped shunt capacitor on the order of femtofarads.

Simulation results at 10 GHz are shown in Fig. 7. The CPW center conductor width is $w = 60$ μm and the gapwidth is $s = 40$ μm. The substrate is modeled after silicon ($\varepsilon_{rs} = 11.7$) and the metal is modeled with perfect-electric-conducting surfaces. The probe dimensions are 500 μm $\times$ 500 μm $\times$ 200 μm and its relative dielectric constant is $\varepsilon_{rp} = 12.9$ (GaAs). The graded-index lens is patterned after bulk borosilicate glass ($\varepsilon_{rl} = 2.5$) and has a diameter of 1 mm and a length of 2.5 cm. At a height of 25.4 μm (one full notch on a physical micrometer knob), Z_o decreases by 19% and the full-width at half-maximum of the perturbation is 0.5 mm. Hence, the electromagnetic disturbance is essentially localized around the probe. Fig. 8 shows that as the height of the probe decreases the peak characteristic impedance and the peak capacitance per unit length begin to change significantly as the probe comes within 50 μm of the CPW.

Since the probe fills the top region of the transmission line with a high-dielectric constant material, it capacitively loads down the transmission line, resulting in a local change of the capacitance per unit length. Therefore, the effect of the probe can be modeled with a shunt capacitance across an unloaded line. For RF frequencies such that the guide wavelength is much larger than the width of the probe, the average change in the capacitance per unit length taken over the length of the perturbation provides a value for a lumped-element equivalent-circuit shunt capacitance. The equivalent circuit is shown in the inset of Fig. 8, where the shunt capacitance from the probe is denoted $C_{\rm probe}$. The magnitude of $C_{\rm probe}$ is on the order of a few femtofarads.

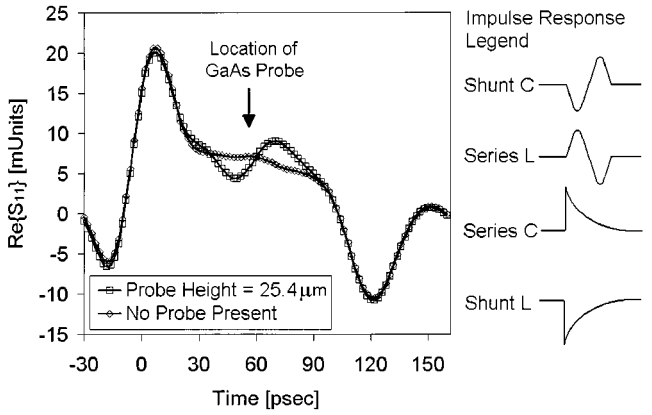

Fig. 9. HP 8510 vector-network-analyzer time-domain (low-pass) measurements of the probe over the CPW. The impulse response verifies the capacitive loading.

B. Measurements of Invasiveness

The full-wave simulations were experimentally verified via time-domain (low-pass) measurements using an HP 8510C Network Analyzer and 150-μm-pitch on-wafer probes. The measured data for a GaAs probe over a CPW transmission line (400-μm-thick silicon substrate, 1-μm-thick gold metallization, 60-μm center conductor, 40-μm gap) is shown in Fig. 9. The center perturbation is the response from the probe and it clearly appears as a shunt capacitance when the probe is 25.4 μm above the line. The two side peaks represent the response from the 150-μm-pitch on-wafer probes.

The effect of the probe on the return loss in the frequency domain is shown in Fig. 10. The effect of a shunt capacitance is to cause the peaks to alternately shift above and below the response from an unperturbed transmission line. Fig. 11 shows simulated data of a CPW line with an additional lumped femtofarad shunt capacitor.[2] The same behavior of shifted peaks is observed, thereby verifying the order of magnitude of the loading capacitance. The return loss changes by 4 dBm at most where it shifts from -34 to -31 dBm. Therefore, the effect of the probe on S_{11} is essentially negligible.

VI. Applications

To demonstrate the usefulness of the electrothermal probe, the thermal and electric fields of a single MMIC cell within an X-band quasi-optical power-combining array were examined. A horn antenna fed an RF signal to an array of patch antennas, which coupled power to a set of amplifying MMICs via microstrip line. The output of each MMIC was re-radiated via an array of patch antennas allowing free-space power combining to be accomplished.

[2]HP EEsof Series IV Libra 6.1, Hewlett-Packard, Santa Rosa, CA, 1997.

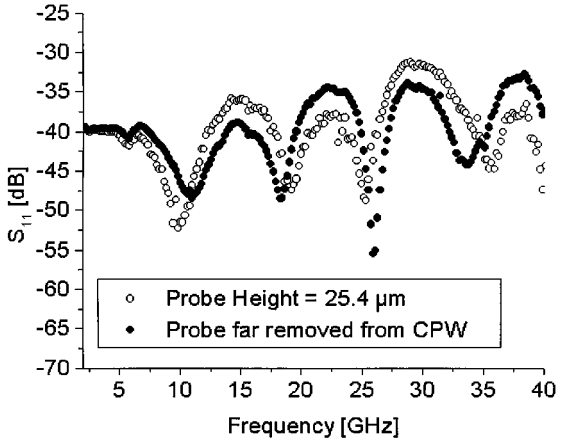

Fig. 10. Frequency-domain measurements (HP 8510) of S_{11} when the probe is over the CPW. The return loss changes by 4 dBm at most where it shifts from -34 to -31 dBm, showing that the effect of the probe is quite minimal.

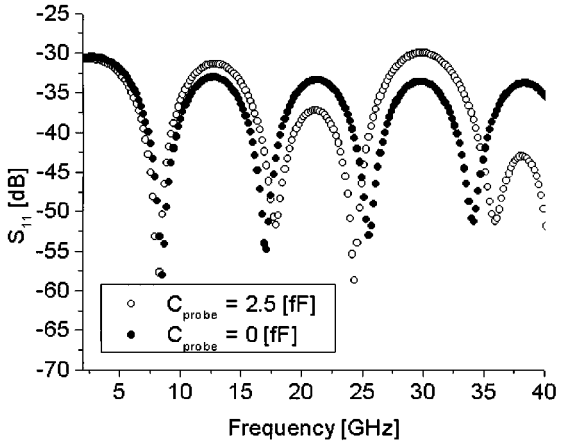

Fig. 11. Simulated data (HP EEsof Libra) of CPW with an additional lumped femtofarad shunt capacitor. The simulation is in good agreement with the measurements of S_{11} (verifying the order of magnitude of the loading capacitance).

The probe was mounted near the output of the MMIC and less than 0.5 mm above the microstrip substrate. For comparison purposes, a power meter was mounted in the far field of the array in order to independently monitor its output performance. To isolate the MMIC under test, the input and output patch antennas for all the other MMICs were covered with copper tape. The bias and RF for the array was switched on at time zero. Fig. 12 clearly shows that there is a substantial difference between the behavior of the measured electric-field data obtained from the probe and the measured power from the independent power meter. The explanation for the discrepancy is shown in Fig. 13 as the absorption data from the probe is seen to decrease with time along with the electric-field data. The change in the absorption signal is consistent with the expected increase in temperature in the vicinity of the biased MMIC due to the dissipation of heat.

Calibration of the temperature effects of the probe on the electric-field measurements is possible since the absorption signal is linearly proportional to the electric-field signal. Knowledge of the deviation of the absorption signal with time $\Delta V_{80\ \mathrm{MHz}}$

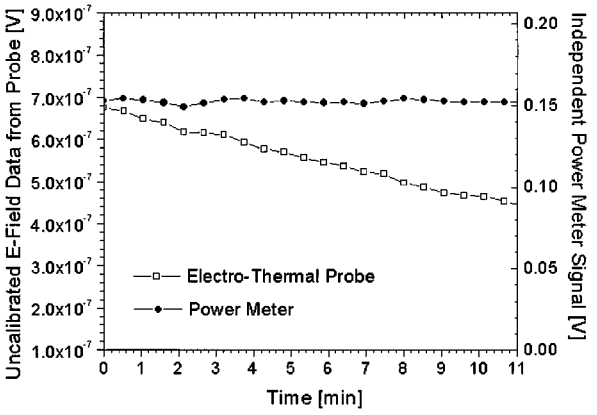

Fig. 12. Probe and power-meter measurement of the MMIC.

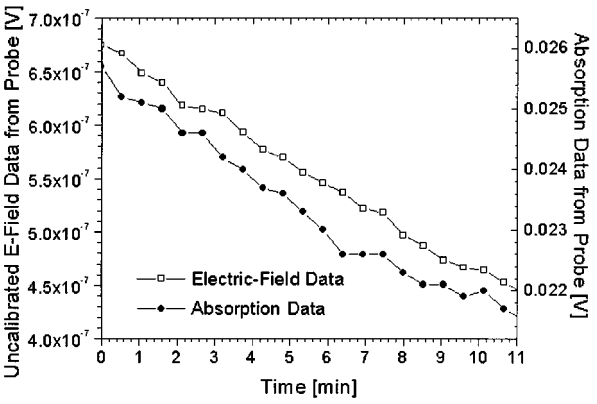

Fig. 13. Probe-only measurements of the MMIC.

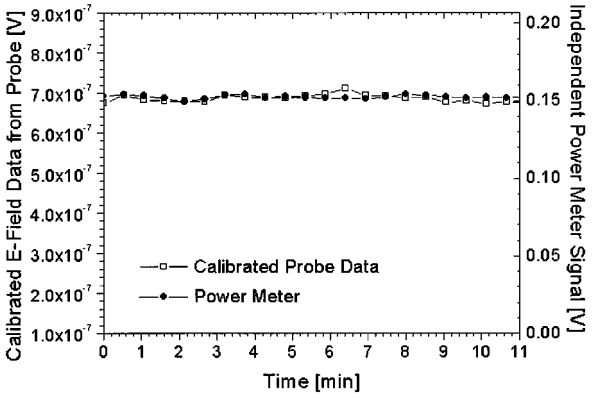

Fig. 14. Temperature-calibrated electric-field data.

allows for the compensation of the modulation signal for temperature effects according to

$$V'_{3\,\mathrm{MHZ}} = \left(\frac{dV_{3\ \mathrm{MHz}}}{dV_{80\ \mathrm{MHz}}}\right)\Delta V_{80\ \mathrm{MHz}} + V_{3\ \mathrm{MHz}} \qquad (11)$$

where the primed notation denotes temperature-calibrated data. The results of this calibration method are shown in Fig. 14. The calibrated electric-field data is now in excellent agreement with the independent power-meter measurements. The calculated standard deviation is 1.3%.

Fig. 15 illustrates the results from the simultaneous data collected from the probe. Knowledge of the initial room tempera-

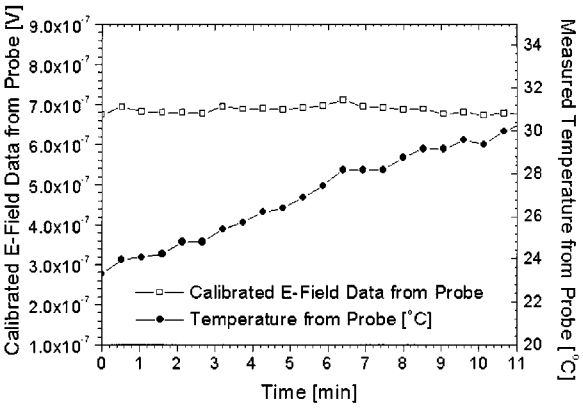

Fig. 15. Simultaneous electric-field and temperature measurements of the MMIC.

ture, the optical-power/temperature relationship, and the deviation of the 80-MHz component with time allow for the scaling of the 80-MHz component to degrees Celsius. The region neighboring the output of the MMIC is seen to increase by 7 °C in 11 min.

VII. Conclusion

An integrated electrothermal probe capable of simultaneously measuring thermal and electric fields has been presented. Experimental observations of the response of the probe to thermal and electric fields are shown to be consistent with theoretical expectations. This novel measurement technique can provide new and fundamental insight into the combined electrothermal behavior of complex active microwave and millimeter-wave structures and allows for the calibration of electric-field data that is corrupted when the probe is used in regions where temperature gradients exist.

Acknowledgment

The authors wish to thank A. Mortazawi, North Carolina State University, Raleigh, for the use of the quasi-optical power-combining array.

References

[1] W. Batty, A. J. Panks, R. G. Johnson, and C. M. Snowden, "Electrothermal modeling and measurement for spatial power combining at millimeter wavelengths," *IEEE Trans. Microwave Theory Tech.*, vol. 47, pp. 2574–2585, Dec. 1999.

[2] H. M. Gutierrez, C. E. Christoffersen, and M. B. Steer, "An integrated environment for the simulation of electrical, thermal and electromagnetic interactions in high-performance integrated circuits," in *IEEE 8th Elect. Performance Electron. Packag. Topical Meeting*, Oct. 1999, pp. 217–220.

[3] R. G. Johnson, C. M. Snowden, and R. D. Pollard, "A physics-based electro-thermal model for microwave and millimeter wave HEMTs," in *IEEE MTT-S Int. Microwave Symp. Dig.*, vol. 3, June 1997, pp. 1485–1488.

[4] N. S. Cheng, P. Jia, D. B. Rensch, and R. A. York, "A 120-W X-band spatially combined solid-state amplifier," *IEEE Trans. Microwave Theory Tech.*, vol. 47, pp. 2557–2561, Dec. 1999.

[5] J. Hubert, L. Mirth, S. Ortiz, and A. Mortazawi, "A 4 watt Ka-band quasi-optical amplifier," in *IEEE MTT-S Int. Microwave Symp. Dig.*, vol. 2, June 1999, pp. 551–554.

[6] K. Yang, L. P. B. Katehi, and J. F. Whitaker, "Electro-optic field mapping system utilizing external gallium arsenide probes," *Appl. Phys. Lett.*, vol. 77, pp. 486–488, July 2000.

[7] S. Wakana, T. Ohara, M. Abe, E. Yamazaki, M. Kishi, and M. Tsuchiya, "Fiber-edge electrooptic/magnetooptic probe for spectral-domain analysis of electromagnetic field," *IEEE Trans. Microwave Theory Tech.*, vol. 48, pp. 2611–2616, Dec. 2000.

[8] A. Yariv and P. Yeh, *Optical Waves in Crystals*. New York: Wiley, 1984.

[9] M. Beaudoin, S. R. Johnson, A. J. G. DeVries, A. Mohades-Kassai, T. Tiedje, R. J. Shul, S. J. Pearton, F. Ren, and C. S. Wu, "Temperature dependence of the optical absorption edge in indium phosphide," in *Compound Semiconduct. Electron. Photon. Symp.*, Apr. 1996, pp. 367–372.

[10] Y. P. Varshni, "Temperature dependence of the energy gap in semiconductors," *Physica*, vol. 34, pp. 149–154, May 1967.

[11] H. C. Casey, D. D. Sell, and K. W. Wecht, "Concentration dependence of the absorption coefficient for n- and p-type GaAs between 1.3 and 1.6 eV," *J. Appl. Phys.*, vol. 46, pp. 250–257, Jan. 1975.

[12] K. Yang, L. P. B. Katehi, and J. F. Whitaker, "Electric-field mapping system using an optical-fiber-based electro-optic probe," *IEEE Microwave Wireless Comp. Lett.*, vol. 11, pp. 164–166, Apr. 2001.

[13] M. Shinagawa and T. Nagatsuma, "Electro-optic sampling using an external GaAs probe tip," *Electron. Lett.*, vol. 26, pp. 1341–1343, Aug. 1990.

[14] R. F. Harrington, *Time-Harmonic Electromagnetic Fields*. New York: McGraw-Hill, 1961.

[15] T. Nagatsuma, T. Shibata, E. Sano, and A. Iwata, "Subpicosecond sampling using a noncontact electro-optic probe," *J. Appl. Phys.*, vol. 66, pp. 4001–4009, Nov. 1989.

[16] D. Conn, X. Wu, J. Song, and K. Nickerson, "A full wave simulation of disturbances in picosecond signals by electro-optic probing," in *IEEE MTT-S Int. Microwave Symp. Dig.* New York, June 1992, pp. 665–668.

[17] K. Yang, G. David, J. G. Yook, I. Papapolymerou, L. P. B. Katehi, and J. F. Whitaker, "Electro-optic mapping and finite-element modeling of the near-field pattern of a microstrip patch antenna," *IEEE Trans. Microwave Theory Tech.*, vol. 48, pp. 288–294, Feb. 2000.

[18] X. Wu, D. Conn, J. Song, and K. Nickerson, "Invasiveness of $LiTaO_3$ and GaAs probes in external E–O sampling," *J. Lightwave Technol.*, vol. 11, pp. 448–454, Mar. 1993.

[19] T. Nagatsuma, T. Shibata, E. Sano, and A. Iwata, "Subpicosecond sampling using a noncontact electro-optic probe," *J. Appl. Phys.*, vol. 66, pp. 4001–4009, Nov. 1989.

[20] M. Y. Frankel, J. F. Whitaker, G. A. Mourou, and A. Valdmanis, "Experimental characterization of external electrooptic probes," *IEEE Microwave Guided Wave Lett.*, vol. 1, pp. 60–62, Mar. 1991.

[21] G. Liang, Y. Liu, and K. Mei, "Full-wave analysis of coplanar waveguide and slotline using the time-domain finite-difference method," *IEEE Trans. Microwave Theory Tech.*, vol. 37, pp. 1949–1957, Dec. 1989.

Ronald M. Reano (S'00) received the B.S. degree in physics from the University of California at Los Angeles, in 1991, the B.S. degree in electrical engineering from the University of New Mexico, Albuquerque, in 1996, the M.S. degree in electrical engineering from The University of Michigan at Ann Arbor, in 2000, and is currently working toward the Ph.D. degree at The University of Michigan at Ann Arbor.

From May 1992 to October 1996, he was with the Air Force Operational Test and Evaluation Center, Kirtland Air Force Base, NM, where he was an Electronic Aircraft Systems Reliability Analyst. His current research interests involve optoelectronic materials and optical measurement techniques for studying microwave and millimeter-wave devices.

Mr. Reano was the recipient of the 2001 First Place Award at the Student Paper Competition presented at the IEEE International Microwave Theory and Techniques Society (IEEE MTT-S) Symposium. He was also the recipient of the 1999 Outstanding Graduate Student Instructor Award presented by the Electrical Engineering and Computer Science Department, University of Michigan at Ann Arbor.

Kyoung Yang (S'90–M'93) was born in Seoul, Korea. He received the B.S. and M.S. degrees in electrical engineering from the Seoul National University, Seoul, Korea, in 1990 and 1993, and the Ph.D. degree in electrical engineering and computer science from The University of Michigan at Ann Arbor, in 2000.

He is currently a Research Fellow with the Electrical Engineering and Computer Science Department, University of Michigan at Ann Arbor. His current research interests include the development and implementations of high-speed electrooptic and photoconductive measurement techniques for the characterization of microwave and millimeter-wave circuits and radiators.

Linda P. B. Katehi (S'81–M'84–SM'89–F'95) received the B.S.E.E. degree from the National Technical University of Athens, Athens, Greece, in 1977, and the M.S.E.E. and Ph.D. degrees from the University of California at Los Angeles, in 1981 and 1984, respectively.

In September 1984, she joined the faculty of the Electrical Engineering and Computer Science Department, The University of Michigan at Ann Arbor, as an Assistant Professor, and then became an Associate Professor in 1989 and Professor in 1994. She has served in many administrative positions, including Director of Graduate Programs, College of Engineering (1995–1996), Elected Member of the College Executive Committee (1996–1998), Associate Dean For Graduate Education (1998–1999), and Associate Dean for Academic Affairs (since September 1999). She has authored or co-authored 410 papers published in refereed journals and symposia proceedings and she holds four U.S. patents. She has also generated 20 Ph.D. students.

Dr. Katehi is a member of the IEEE Antennas and Propagation Society (IEEE AP-S), the IEEE Microwave Theory and Techniques Society (IEEE MTT-S), Sigma Xi, Hybrid Microelectronics, and URSI Commission D. She was a member of the IEEE AP-S AdCom (1992–1995). She was an associate editor for the IEEE TRANSACTIONS ON MICROWAVE THEORY AND TECHNIQUES and the IEEE TRANSACTIONS ON ANTENNAS AND PROPAGATION. She was the recipient of the 1984 IEEE AP-S W. P. King (Best Paper Award for a Young Engineer), the 1985 IEEE AP-S S. A. Schelkunoff Award (Best Paper Award), the 1987 National Science Foundation Presidential Young Investigator Award, the 1987 URSI Booker Award, the 1994 Humboldt Research Award, the 1994 University of Michigan Faculty Recognition Award, the 1996 IEEE MTT-S Microwave Prize, the 1997 International Microelectronics and Packaging Society (IMAPS) Best Paper Award, and the 2000 IEEE Third Millennium Medal.

John F. Whitaker (S'84–M'88) received the B.Sc. degree in physics from Bucknell University, Lewisburg, PA, in 1981, and the M.Sc. and Ph.D. degrees in electrical engineering from the University of Rochester, Rochester, NY, in 1983 and 1988, respectively.

In 1989, he joined the faculty of the Department of Electrical Engineering and Computer Science, The University of Michigan at Ann Arbor, where he is currently a Research Scientist and Adjunct Professor and Coordinator of the Ultrafast Technology Area in the National Science Foundation (NSF) Center for Ultrafast Optical Science. In 1995, he was a Visiting Professor, First Class, at the University of Savoie, Savoie, France. His research interests involve ultrafast-response optoelectronic materials, devices, and test and characterization techniques, as well as guided and free-space-radiating terahertz-bandwidth pulses.

Dr. Whitaker is a member of IEEE Microwave Theory and Techniques Society (IEEE MTT-S) and the IEEE Lasers and Electro-Optics Society (IEEE LEOS). He was the recipient of the 1996 Microwave Prize presented by the IEEE MTT-S. He was also the recipient of the Research Excellence Award presented by the Department of Electrical Engineering and Computer Science, the Outstanding Research Scientist Achievement Award from the College of Engineering, and the Research Scientist Recognition Award from the Office of the Vice President for Research, all from The University of Michigan at Ann Arbor.